13th ewtec 2019 Proceedings of the 13th European Wave and Tidal Energy Conference 1-6 Sept 2019, Naples, Italy

CCP-WSI blind test 2: Modelling focused wave interactions with floating structures with WEC-Sim

Jack Hughes, Alison Williams and Ian Masters

***Abstract*—Efficient modelling of wave-structure interactions is important in understanding system behaviour and performance of marine energy devices over a range of conditions. Focused waves are typically applied as an effective representation of extreme waves, when compared with regular or random wave methods. In this paper, CCP-WSI Blind Test 2 experiments are modelled in open source wave energy converter dynamics modelling software, WEC-Sim in which two surface-piercing, linearly elastically moored floating buoys were subject to a series of focused waves. Buoy motions and hydrodynamic forces are modelled in the time domain using linear frequency domain hydrodynamic coefficients estimated by a boundary element method. In lieu of experimental results for comparison, the WEC-Sim results have been compared with a similar experimental study which appear to show good performance in predicting wave induced motions from the WEC-Sim model in some directions but not others which may be due to the presence of nonlinear fluid-structure interactions unaccounted for in the model. WEC-Sim is computationally faster than CFD methods at the expense of nonlinear interactions. Therefore, this blind test will help to quantify this trade off.**

***Index Terms*—CCP-WSI, wave-structure interactions, WEC-Sim**

I. Introduction

THE CCP-WSI Blind Test Series involves experimental and numerical modelling of focused wave interactions with floating bodies, though only the properties of the experimental setup are disclosed at the beginning of the campaign [1]. The experimental campaign was carried out in the COAST laboratory ocean basin and involved subjecting two cylindrical geometries, one with hemispherical bottom and the other with a cylindrical moon-pool in the centre, to a series of focused waves, generated using the NewWave theory.

Focused waves can effectively represent the energy of the largest extreme waves at a known time and location [2], offering benefits over random wave generation or regular waves which fail to describe the extreme waves or are extremely time consuming due to the stochastic nature of extreme events.

WEC-Sim [3] is a simulation tool for modelling wave energy converters (WEC), which uses a radiation and diffraction method to determine operational motions and loads of WECs in the time domain. This method relies on frequency domain boundary element method (BEM) solvers, such as WAMIT and NEMOH, to provide hydrodynamic coefficients as inputs to the model. Linear potential flow theory, used in BEM, relies on a number of assumptions which can be limiting when considering wave events with the presence of higher order effects.

Despite the known limitations of linear potential flow theory based models, the large improvements on computational power and time required to model time domain hydrodynamics and system dynamics of marine renewable energy devices when compared with higher order and fully nonlinear models such as CFD, makes software like WEC-Sim very valuable in the early stages of the design phase. Modelling the CCP-WSI experiments in WEC-Sim will provide a parametric understanding into the effect of wave steepness and the varying effect it has on the reliability of the model, which is particularly useful for recognising when is appropriate to apply linear modelling tools. A clear understanding of the boundaries of accuracy of these models allows an informed choice between efficiency and computational effort needed for CFD approaches.

Quon et al. [4] use nonlinear features in WEC-Sim to predict the most likely extreme response (MLER) of a floating point absorber WEC. The MLER method is used to elicit the maximum response of a floating body in a specified degree of freedom, thus a focused wave is generated based on extreme wave statistics and the linear response amplitude operator (RAO) in the degree of freedom of interest computed in WEC-Sim. It is assumed that the nonlinear response of a floating body can be approximated by a linearised solution, with the solution deviating only slightly from the nonlinear response.

In this paper a description of the blind test experimental series is given, before the underlying theoretical aspects and methodology of NEMOH and WEC-Sim are detailed. Timeseries motions and forces of the two geometries are presented with a discussion of the findings.

Paper ID: 1450. Track: Wave hydrodynamic modelling. This work represents the authors participation in the CCP-WSI Blind Test Series 2. This work was supported in part by the Swansea University College of Engineering PhD studentship and the SURFTEC project, funded by EPSRC under grant EP/N02057X/1.

J. Hughes is at the Energy and Environment Research Group, Swansea University Bay Campus, Fabian Way, Skewen, Swansea, SA1 8EN (e-mail: 708774@swansea.ac.uk).

A. Williams is at the Energy and Environment Research Group, Swansea University Bay Campus, Fabian Way, Skewen, Swansea, SA1 8EN (e-mail: Alison.J.Williams@swansea.ac.uk).

I. Masters is at the Energy and Environment Research Group, Swansea University Bay Campus, Fabian Way, Skewen, Swansea, SA1 8EN (e-mail: I.Masters@swansea.ac.uk).

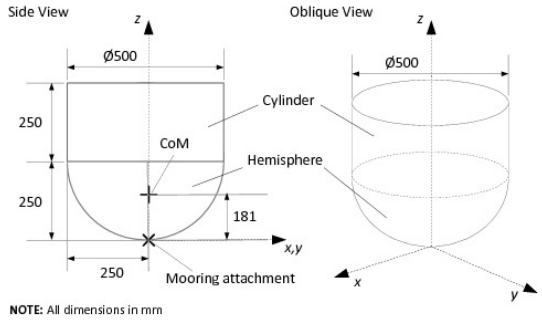

Fig. 1. Geometry 1: Hemispherical-bottomed cylinder (all dimensions in mm) [1]

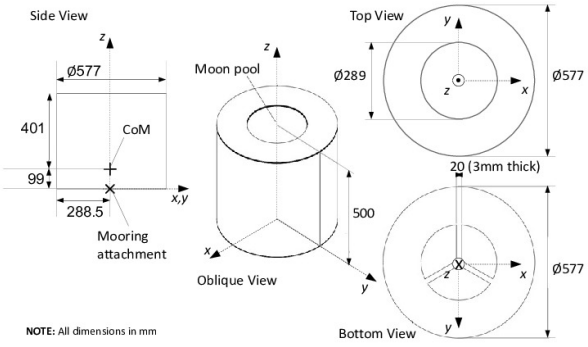

Fig. 2. Geometry 2: Cylinder with moon-pool (all dimensions in mm) [1]

II. Description of Experiments

The first geometry is a hemispherical-bottomed cylinder, moored at a single point at the bottom-most point of the hemisphere on the axial line as shown by the 'x' in Fig. 1.

The second geometry is a cylinder with a central, cylindrical moon-pool, which introduces additional complexity with an 'internal' body of water. This geometry is also moored at a single point on an additional frame which allows the mooring attachment to be located at level with the bottom of the cylinder on the axial line, shown by the 'x' in Fig. 2.

The experiments performed at the COAST laboratory consisted of generating the incident waves in the ocean basin with and without the buoys present. Generating the wave in the absence of the buoys allowed for undisturbed wave surface elevation measurements using an array of wave gauges and producing surface elevation data for use in and comparison with computational models.

In addition to wave gauge measurements, the motion of buoys was tracked and the mooring load was measured in the single point, linearly elastic taut mooring line using a load cell.

Three incident waves were generated at the COAST laboratory and subsequently subjected upon the buoys individually. Each wave was created using linear superposition of 244 wave fronts at a theoretical focus location with frequencies evenly spaced between 0.101563 Hz and 2 Hz. This was acheived by applying the NewWave theory to a Pierson-Moskowitz spectrum

TABLE I
Wave parameters for CCP-WSI test cases [1]

CCP-WSI ID	A_n	f_p	h	H_s	kA
	(m)	(Hz)	(m)	(m)	-
1BT2	0.25	0.3578	3.0	0.274	0.128778
2BT2	0.25	0.4	3.0	0.274	0.160972
3BT2	0.25	0.4382	3.0	0.274	0.193167

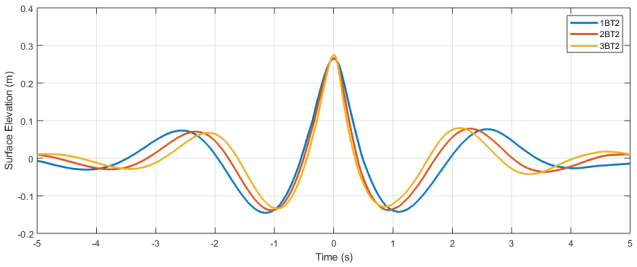

Fig. 3. Surface elevation measurements from empty tank tests and artificially aligned at $t = 0$ [1]

to derive the amplitudes of frequency components using the parameters in Table I where a_n is the amplitude of Fourier series coefficient n, f_p is the peak frequency, h is the water depth, H_s is the significant wave height and kA is the wave steepness. The waves described are all crest-focused, meaning that the phase angle would be zero at the focus location. Fig. 3 shows the surface elevation measurements taken at the resting position of the geometries for each of the waves described in Table I during the empty tank tests.

III. Theory

A. NEMOH

BEM software, NEMOH, has been developed at École Centrale de Nantes as an open source alternative to commercial BEM codes such as WAMIT, using a linear frequency domain potential flow theory based numerical model [5].

NEMOH has benefited multiple offshore industries and its applications include estimating the dynamic response of floating structures and performance assessment of WECs. Its outputs include first order hydrodynamic coefficients; added mass, radiation damping and excitation force, far field coefficients from the Kochin function, free surface elevation and pressure field [6].

In a study by Penalba et al. [7], the added-mass, radiation damping and excitation force coefficients generated in Nemoh were found to agree well with those generated in WAMIT, with the exception of models including thin elements and the removal of uncharacteristically high amplitudes of some frequency components, referred to as irregular frequencies by the NEMOH community. However, this only typically affect results at high wave frequencies.

Linear potential flow theory is applied to solve first order hydrodynamic coefficients in the frequency domain, which relies on the following assumptions [3], [6]:

1) The flow is inviscid.
2) The fluid is incompressible.

3) The wave amplitude is small, with regards to the wavelength.
4) The amplitude of the body motion is small with respect to its dimension.
5) The seabed is flat.

The validity of applying linear wave theory when considering extreme wave events, i.e. large displacements and steep waves, presents issues with assumptions 3 and 4. The validity of various wave theories dependant on steepness and depth is realised by Le Méhauté in 'An Introduction to Hydrodynamics and Water Waves' [8], in which, as wave steepness increases, the validity of linear wave theory decreases and higher-order terms must be considered as the assumption that linear effects are much larger than higher order effects breaks down [9].

NEMOH uses a constant panel method in which the wetted surface of the body is discretised in flat panels, which assumes that the velocity potential and its normal derivative are constant over the panels of the mesh [6]. The use of flat panels is limiting for curved and complex geometries, especially within the NEMOH mesh limit of approximately 3,000 elements.

B. WEC-Sim

The frequency domain hydrodynamic coefficients generated in NEMOH are output to BEMIO; a WEC-Sim pre- and post-processor code in which Impulse Response Frequencies (IRFs) are calculated and converted to a useful format for use in WEC-Sim.

WEC-Sim solves the WEC dynamics in the time domain via the equation of motion about the centre of gravity of the floating body and is a combination of force and torque vectors, comprised of translational and rotational components [3]:

$$m\ddot{X}(t) = F_{exc}(t) + F_{rad}(t) + F_{PTO}(t) + F_v(t) + F_{ME}(t) + F_B(t) + F_m(t) \quad (1)$$

where m is the mass matrix, $\ddot{X}$ is the acceleration vector of the device, F_{exc}, F_{rad}, F_{PTO}, F_v, F_{ME}, F_B and F_m are the excitation, radiation, power take-off (PTO), damping, Morison elements, net buoyancy and mooring force and torque vectors, respectively.

In its simplest form, WEC-Sim creates a linear model and calculates F_{exc}, F_{rad} and F_B of a floating body subject to incident waves using frequency domain hydrodynamic coefficients, with the remaining terms neglected unless specified using assumptions 1 - 5 [3]. A convolution integral method is used to represent fluid memory effects on the floating body. Complexity may be added to the model with options to model viscous effects, custom power take-off systems and mooring configuration.

Excitation and radiation damping forces, F_{exc} and F_{rad}, of the body can be calculated using a sinusoidal steady-state method, or via a convolution integral method which generates fluid memory retardation forces. Excitation force is calculated based on the free surface profile at the centre of mass of the body:

$$F_{exc}(t) = \Re\left[\frac{1}{2}R_f H F_{exc}(\omega,\beta)e^{i(\omega t)}\right] \quad (2)$$

where R_f is the ramp function, used to eliminate strong transient flows early on in the simulation, H is the wave height, F_{exc} is the frequency dependent complex wave excitation amplitude vector and β is the wave heading.

The time domain radiation damping force is obtained using frequency domain added mass and radiation damping terms, A and B:

$$F_{rad}(t) = -A(\omega)\ddot{X} - B_\omega\dot{X} \quad (3)$$

where $\dot{X}$ is the velocity vector.

The linear net buoyancy forces are calculated based on the displaced volume of the buoy:

$$F_B(t) = \rho g V \quad (4)$$

where ρ is the water density and g is the gravitational constant.

Modelling the linearly elastic mooring line in WEC-Sim can be achieved through WEC-Sim's built-in mooring matrix, or external lumped-mass mooring line model, MoorDyn. The mooring matrix method is applied in this work and uses the equation:

$$F_m = -K_m X - C_m\dot{X} \quad (5)$$

to solve the translational and rotational stiffness where K_m and C_m are the stiffness and damping matrices for the mooring system, respectively and X is the displacement vector of the body.

WEC-Sim includes the F_v term in the equation of motion to introduce viscous damping effects, which would otherwise be neglected as per assumption 1 of the BEM solver, which is defined as:

$$F_v = -C_v\ddot{X} - \frac{1}{2}\rho C_D A_D \dot{X}|\dot{X}| \quad (6)$$

where C_v is the linear damping coefficient, ρ is the fluid density, C_D is the viscous drag coefficient and A_D is the characteristic area. Though in reality C_D varies dynamically with Reynolds number, it is defined within WEC-Sim as a constant and the best representative value should therefore be chosen based on the geometry.

A weakly nonlinear approach can be applied in WEC-Sim to account for nonlinear buoyancy and Froude-Krylov wave excitation force contributions [3]. This approach does not use BEM calculated linear wave excitation and hydrostatic coefficients, but rather integrates the theoretical static and dynamic pressures over each panel of the mesh along the wetted body surface at each time step. Wheeler stretching [10] is applied to satisfy the boundary condition at the water surface based on the instantaneous wave elevation. The nonlinear features, however, are not intended for modelling highly nonlinear events such as wave slamming and wave breaking [3].

IV. METHODS

C. NEMOH

Frequency domain hydrodynamic coefficients for Geometry 1 and 2 were generated in NEMOH based on a user-defined frequency range with a wave heading of 0°. A mesh sensitivity study was conducted

TABLE II
NEMOH MESH SENSITIVITY RESULTS OF MAX A AND B VALUES FOR GEOMETRY 1 AND 2

Mode	Mesh	Geometry 1 A_{max}	Geometry 1 B_{max}	Geometry 2 A_{max}	Geometry 2 B_{max}
Surge	1	4.13E+04	5.84E+04	1.15E+05	1.33E+05
	2	3.99E+04	5.66E+04	1.15E+05	1.06E+05
	3	3.88E+04	5.54E+04	1.17E+05	1.03E+05
	4	3.80E+04	5.45E+04	1.15E+05	1.01E+05
Heave	1	2.47E+04	1.06E+04	3.25E+04	1.34E+05
	2	2.67E+04	1.16E+04	3.13E+04	1.07E+05
	3	2.75E+04	1.21E+04	3.11E+04	2.11E+05
	4	2.77E+04	1.22E+04	3.04E+04	7.94E+04

to determine a suitable output for use in WEC-Sim, in which multiple meshes were produced in CAD software, Salome, based on the geometries.

For surface-piercing geometries, such as those used in the CCP-WSI campaign, the NEMOH mesh only includes the wetted surface and thus any section of the geometry above the still water line (SWL) are excluded.

Issues arose with radiation damping force calculations when generating NEMOH results using the original dimensions, which resulted in undamped, freely oscillating geometry motions in WEC-Sim. This is related to spatial tolerances within NEMOH that appear when modelling small (tank testing scale) geometries. A work around this was acheived by applying a Froude scaling factor of $\lambda = 10$ to the NEMOH and WEC-Sim models, before scaling down the results was found to resolve this issue without damaging the results. Froude scaling has been applied based on the SUPERGEN's 'Guidance for the experimental tank testing of wave energy converters' [11].

The frequency range in NEMOH, which uses rad/s as frequency units, was based on the frequency range of wave fronts used to produce the focused waves, i.e. between 0.101563 Hz and 2 Hz. For the Froude scaled NEMOH computation the frequency scale factor was $\lambda^{-0.5}$. Similarly, the sea depth in NEMOH was scaled by a factor λ based on the ocean basin depth of 3m.

For each geometry the peak added mass and radiation damping values were compared in surge and heave modes. As the geometries are surface piercing the results are susceptible to irregular frequencies [6], which are often large spikes that deviate from the added mass and radiation damping curves. Table II shows the max A and B value variation between meshes obtained for each geometry. The mesh sizes used ranged between 164 and 2180 elements for Geometry 1 and between 492 and 2339 elements for Geometry 2.

With the exception of the B values for geometry 2, all results between mesh 3 and 4 agreed within 2% for maximum A and B values. The time taken to run these meshes was approximately 30 minutes for mesh 3 and over 2 hours for mesh 4.

As mesh size increased, the size of irregular frequencies decrease which is beneficial in alleviating issues in the time domain WEC-Sim model.

Fig. 4 shows the the radiation damping curve for Geometry 2, in which a prevalent spike at a wave

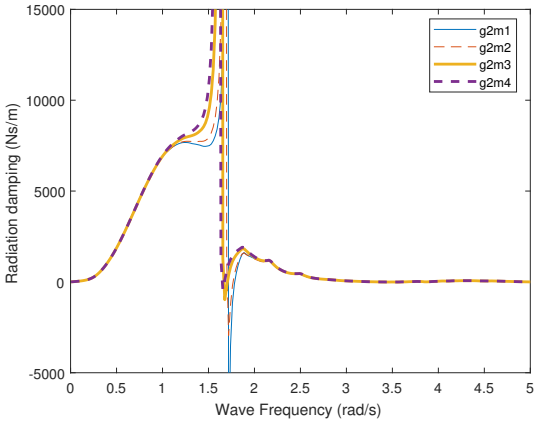

Fig. 4. Mesh sensitivity results for heave radiation damping curve, B, for Geometry 2.

frequency of 1.61 rad/s is clear. Penalba et al. [7] demonstrate a similar phenomenon with a moonpool geometry which may indicate the 'moonpool resonance frequency'.

Ultimately, the selected meshes were Mesh 3 for Geometry 1 and Mesh 4 for Geometry 2. Despite the additional run time for Mesh 4 for Geometry 2, Mesh 3 shows a spuriously high B_{max} result when compared with meshes 1, 2 and 3.

With the presence of large irregular frequencies, the aim of the NEMOH mesh sensitivity is ultimately reduce the impact that these will have on WEC-Sim results. Otherwise, the even the coarsest meshes generally agree well in other areas, as can be seen at below 1 rad/s and above 2 rad/s in Fig. 4.

D. WEC-Sim

There are multiple options for defining waves in WEC-Sim, i.e. regular waves or random sea, depending on the desired conditions. Different numerical methods can be applied in WEC-Sim based on these options.

The method applied in this study uses a predefined timeseries of surface wave elevation, η, typically derived from experimental studies. In this case the surface wave elevation at wave gauge 5 of the empty tank tests [1] has been Froude scaled by a factor of $\lambda = 10$ and applied to the model, as per the Froude scaled hydrodynamic coefficients from NEMOH.

Inconsistencies between the true displaced volume of the geometries and the NEMOH mesh, due to mesh resolution, can present issues in generating a stable WEC-Sim model. The consequences of which are instabilities in the buoyancy equilibrium equation used by WEC-Sim:

$$F_{buoyancy} = F_{gravitational} + F_{pretension} \tag{7}$$

which causes a sudden displacement of the buoy at $t = 0$ due to an imbalance between the mass of the buoy, based on the experimental value, and the mooring pretension and buoyancy force, which is based on the displaced volume. This was corrected by replacing the displaced volume value in NEMOH with a value

calculated based on the experimental displaced volume of the geometries at rest.

The vertical linear mooring stiffness matrix in WEC-Sim is applied in the y direction at the mooring location for each geometry. The experimental mooring stiffness, $k = 67$ N/m, was Froude scaled in the WEC-Sim model by a factor of λ^2 and pretension by a factor of λ^3, as per the scaling guidance [11].

Viscous forces are modelled by supplying a drag coefficent, C_D, and characteristic area in x, y and z. The drag coefficients were obtained through a mixture of CFD and using empirical data. CFD drag coefficients were generated for Geometry 1 using a steady state OpenFOAM model, which was based on the maximum velocity of the buoy in an undamped control decay test simulation in WEC-Sim. Surface characteristics were defined using a wall function, aiming for a y^+ value of less than 30. A $k-\omega$ SST turbulence model was used and the model mesh contained 1.8×10^6 cells, which took approximately 15 minutes to run on a High Performance Computer running 28 cores. However, after the first WEC-Sim simulation the viscous drag contributions were found to be small, so empirical drag coefficients were used for Geometry 2.

Once suitable stability had been achieved for Geometry 1 and 2 with no waves, the timeseries surface wave elevation for waves 1, 2 and 3 were applied to the model using a 0.025 s time-step, which was found to be small enough to maintain a high resolution representation of the input waves without having a negative impact on the overall run time.

E. CCP-WSI Submission Criteria and Spectral Analysis

Appendix A includes the numerical data submitted as part of contributing to CCP-WSI Blind Test Series 2. The maximum values, preceding trough depths and rising times of heave and surge displacement, pitch angle and mooring load were calculated from the timeseries WEC-Sim output within the specified time period, 35.3 s to 50.3 s.

Spectral analysis was performed on the data in this range. A single-sided variance density spectrum was generated using a Fourier transform of the timeseries data. Included in Appendix A are the peak frequency, single-sided variance density and the spectral bandwidth of heave and surge displacement, pitch angle and mooring load.

V. Results

Timeseries results of heave, surge and pitch motions and mooring load over the period from 35.3 seconds to 50.3 seconds are presented here at experimental scale for waves 1BT2, 2BT2 and 3BT2 for each geometry. All results are given about the centre of mass of the relevant geometry. Additionally force contributions are included. Pitch motions are presented according to the left-hand rule. Appendix A contains results submitted to CCP-WSI.

TABLE III
Processing Times of NEMOH, CFD and WEC-Sim for Geometry 1 and 2

Process	Time (mins)	
	Geom 1	Geom 2
NEMOH	30	30
CFD, C_D	15	-
WEC-Sim	2	2
Total	47	32

F. Processing Time

Table III shows the approximate processing times to achieve time domain results from WEC-Sim for each geometry. The NEMOH and WEC-Sim steps were carried out on a standard desktop configuration, whereas the CFD step was carried out using a High Power Computer. It can be seen that the majority of processing time is contributed by NEMOH, which unfortunately cannot be run as parallel processes. Additional time could have been saved for Geometry 1 by using empirical data for the drag coefficients.

G. Geometry 1

Motions and mooring load induced by the waves 1-3BT2 calculated in WEC-Sim are shown in Fig. 5.

In Fig. 5a, the largest upward heave response (z-displacement) is induced by 1BT2, which coincides with the main wave crest at 45.2 s. Conversely, the largest following trough is induced by 3BT2.

The largest surge response is produced by 1BT2 and can be seen in Fig. 5b. Its peaks are offset from heave and wave elevation, which is clear in Fig. 6. The largest negative and positive displacements correspond to the buoy rising and descending from the main crest of the waves.

As wave steepness increases, from wave 1BT2 to 3BT2, the pitch response also increases. The maximum pitch angles of Geometry 1 for waves 1BT2, 2BT2 and 3BT2 are 28°, 33°and 38°, respectively.

The mooring load reflects the heave motions like-for-like, due to the mooring stiffness matrix method which solves the directional mooring load using Eq. 5. Hence, as the mooring line is vertical, stiffness was only calculated in the z direction. However, with measurable surge and pitch motion, the mooring is likely to experience more complex loading than currently accounted for by the mooring matrix, which is currently based only on the heave motions of the buoys.

Forces calculated in WEC-Sim for surge, heave and pitch degrees of freedom are shown for wave 1BT2 in Fig. 7. Wave excitation force has significant contribution to the total force in each case as the focused wave group passes.

In heave (Fig. 7a the excitation and restoring forces act in opposing directions for the majority of the timeseries, resulting in a total force of much smaller magnitude. As the force plot does not include mooring load, the restoring force supplies the total force before the focused wave passes as it opposes the pretension applied to the mooring line, at 32.2 N.

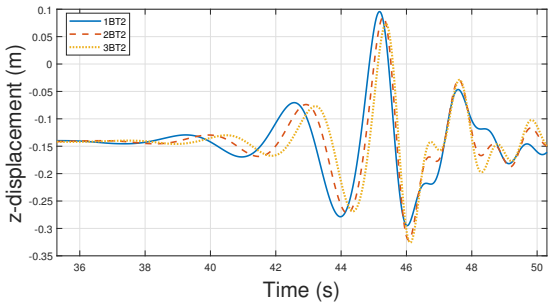

(a) Heave displacement

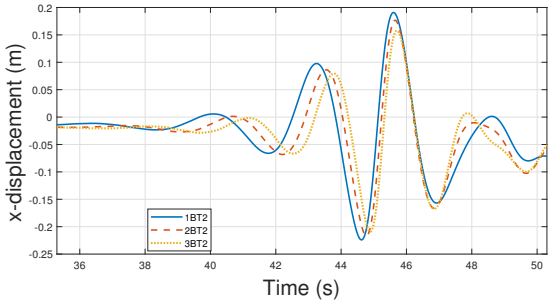

(b) Surge displacement

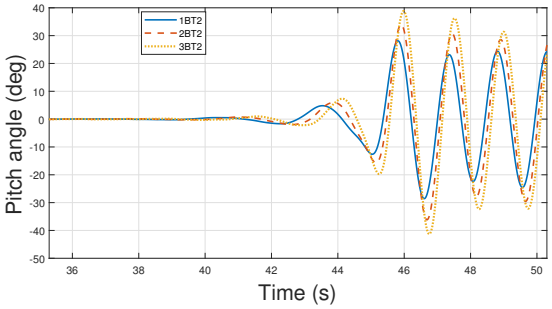

(c) Pitch displacement

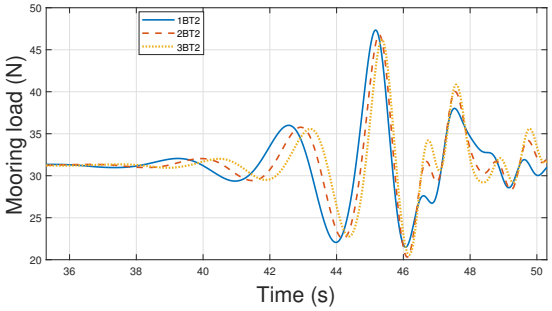

(d) Mooring Load

Fig. 5. Timeseries results showing heave (z) displacement, surge (x) displacement, pitch angle and the mooring load of Geometry 1 when subjected to focused wave groups 1BT2, 2BT2 and 3BT2 calculated in WEC-Sim.

In surge (Fig. 7b), other notable force contributions come from radiation damping and added mass forces, while restoring and viscous forces are negligible.

Pitching motions are initiated by a large excitation force as the main wave crest passes the geometry in Fig. 7c. As the wave group passes, the excitation forces give way to restoring forces which are largest when pitch angle is greatest.

H. Geometry 2

Fig. 8 shows timeseries results of the resulting motions and forces of Geometry 2 when subjected to each

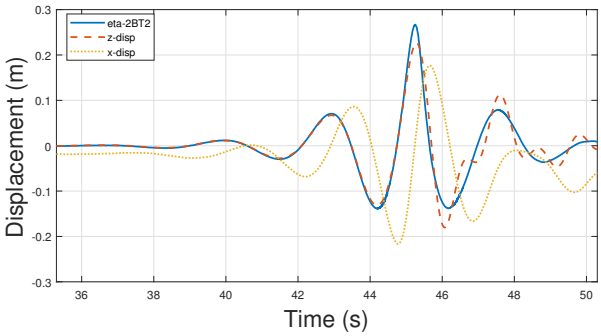

Fig. 6. Timeseries comparison of wave surface elevation of wave 2BT2, η, with heave (z) and surge (x) displacement calculated in WEC-Sim.

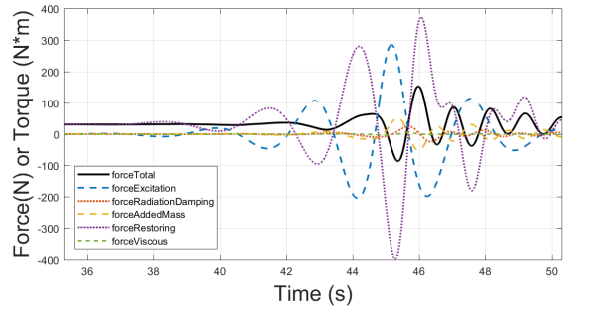

(a) Heave forces

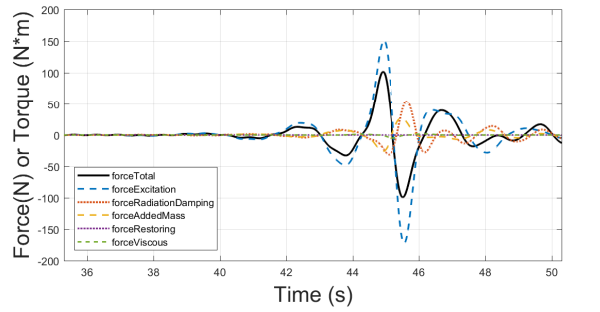

(b) Surge forces

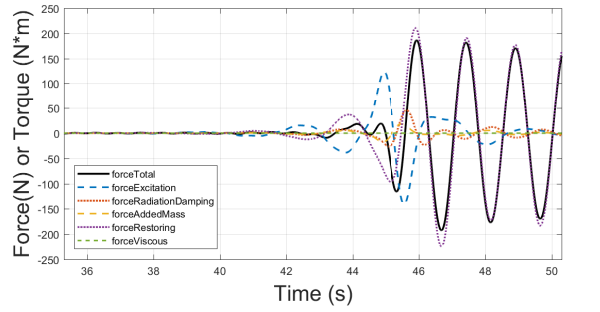

(c) Pitch forces

Fig. 7. Timeseries of force contributions for Geometry 1 when subjected to focused wave (2BT2) calculated in WEC-Sim.

focused wave. Fluctuations are visible in the heave displacement timeseries before the focused wave passes which may be an artefact of irregular frequencies in the NEMOH results for Geometry 2.

In general, a similar pattern emerges between the heave and surge results of Geometry 1, in that the inflection as the buoy rises following the passing of the focused wave group between 47 and 48 seconds in

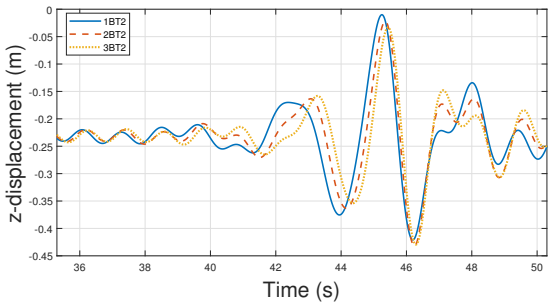

(a) Heave displacement

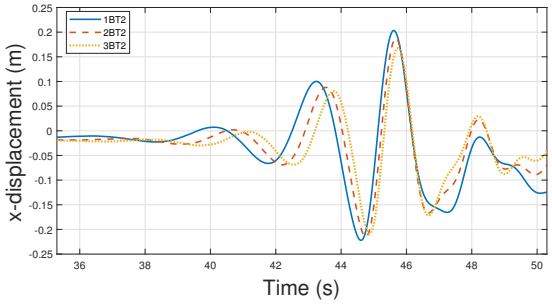

(b) Surge displacement

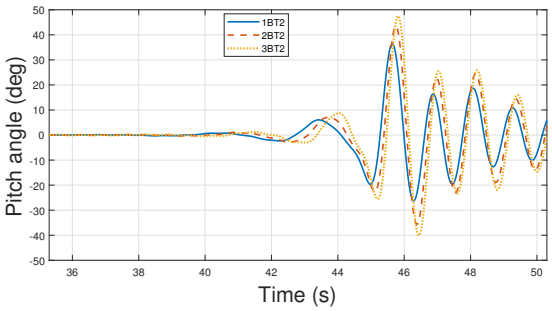

(c) Pitch displacement

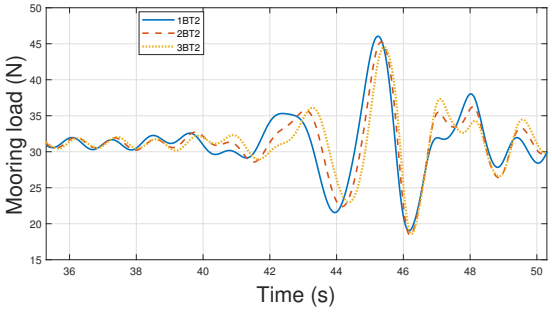

(d) Mooring Load

Fig. 8. Timeseries results showing heave (z) displacement, surge (x) displacement, pitch angle and the mooring load of Geometry 2 when subjected to focused wave groups 1BT2, 2BT2 and 3BT2 calculated in WEC-Sim.

Fig. 8a corresponds to a change in direction of surge motion at the same time in Fig. 8b.

Pitching motions of Geometry 2 appear damped when compared with those of Geometry 1, which may arise due to the presence of the moonpool effects. The added geometrical complexity is likely to manifest itself in errors spanning from the constant panel method of NEMOH calculation which are input to WEC-Sim, where buoy motions appear to be spurious due to the model instabilities.

Again, the mooring load follows the heave motions of the geometry.

VI. Discussion

Comparing the main crest heights in the motions of the geometries shows that the largest surge and heave displacements are induced by wave 1BT2, followed by 2BT2 then 3BT2, despite all input wave surface elevations showing the same crest height. The differences, however are relatively small. Pitch angle shows the contrary, and notable differences are visible between each wave, with wave 3BT2 showing producing the largest pitch angle for both geometries, followed by 2BT2 then 1BT2. Whilst the main crest height of the wave remains the same, the steepness increases from wave 1BT2 to 3BT2 which suggests that the steepness of the wave has a much larger effect on the pitch motions than the surge and heave motions.

Fig. 6 is a time series of wave surface elevation, heave displacement and surge (x) displacement of Geometry 1 when subjected to 2BT2. The heave motions of the buoy follow the wave surface elevation closely with the exception of inflection in heave at approximately 46.5 s, which coincides with a change in direction of surge motion. Due to the uncoupled calculations of motions in WEC-Sim, it is these complex interactions where the authors expect the WEC-Sim model to diverge the most from the experimental results.

Fig. 7 shows minimal viscous force contributions, which suggests that the use of empirical drag coefficients would not negatively affect the overall results. The consequence of using WEC-Sim's method for modelling drag with a constant drag coefficient is likely to manifest itself as a poor representation of the viscous forces, particularly in highly unsteady cases such as the CCP-WSI experiment.

In a similar experimental study, Ransley et al. [12] recorded the focused wave induced motions of a buoy with almost identical geometrical and mass properties to Geometry 1. The focused wave was generated based on the NewWave theory using a Pierson-Moskowitz spectrum with peak frequency, $f_p = 0.356$ Hz, which is similar to wave 1BT2. While the wave properties may not be identical to any of those in this study, the induced experimental motions may be compared with those in this CCP-WSI study for a basis of judgement on WEC-Sim's performance in lieu of experimental results from the CCP-WSI experimental campaign.

In general there are visible similarities in results, particularly heave motions which tend to follow the surface wave elevation. Geometry 1 and the geometry used in the Ransley et al. experiment rest at similar positions in the study with the CoM around -0.141 m. The maximum heave displacement recorded in the experiment is approximately 0.12 m, and in WEC-Sim is 0.10 m for 1BT2.

The surge displacement predicted by WEC-Sim does not achieve a similar magnitude to the experimental results, with the peak WEC-Sim displacement at approximately 0.19 m for 1BT2 and more than 0.4 m in the Ransley et al. experiment. Conversely, the pitch motions appear much larger than the experimental values. This could be due to the exclusion of nonlinear buoy-

ancy forces and meshing limitations in NEMOH that exclude non-wetted sections of the geometry at rest, which are particularly important when considering large displacement scenarios. Dynamic representation of the wetted surface area in the model would result in damped pitch motions from pressure and restoring forces.

The WEC-Sim method has some limitations, in that it is not possible to compute Morison elements or nonlinear hydrodynamics when importing a timeseries of surface wave elevation [3]. Further work will include applying nonlinear WEC-Sim functionality with focused waves as in Quon et al. [4], where the addition of Froude-Krylov forces and nonlinear buoyancy based on the instantaneous wave surface elevation were found to effectively capture weakly non-linear wave-body interactions, offering an improvement on the model presented here. For small geometries, instabilities can arise in the calculation of radiation damping values in NEMOH. This necessitates the use of Froude scaling, which can be done with little consequence for linear models but scaling effects and issues may arise with the computation of nonlinear hydrodynamics in future models.

The WEC-Sim results for Geometry 2 are generally similar to Geometry 1, with the exception of different pitch motion behaviour for all wave cases. Unlike Geometry 1, the pitch motions for Geometry 2 appear damped following the peak angle on the first oscillation. The peak values can be found in Appendix A.

Fluctuations in heave displacement for Geometry 2 begin at the start of the simulation, which may arise due to the instabilities in the frequency dependent complex wave excitation amplitude vector that WEC-Sim relies on to calculate the time domain excitation force in Eq. 2. The NEMOH results for Geometry 2 were susceptible to large irregular frequencies and odd spikes, which may have impacted the quality of the results.

VII. Conclusions

Overall, modelling the CCP-WSI Blind Test 2 using open source, low- to mid-fidelity modelling tools NEMOH and WEC-Sim appeared to show some promising results despite the large displacement limitations of linear potential flow models. Based on a comparison with previous similar experiments, WEC-Sim's calculation of surge displacement and pitch angle are expected to be under and overpredicted, respectively. This is thought to arise due to meshing constraints in NEMOH and the exclusion of weakly nonlinear hydrodynamic forces in WEC-Sim. Predictably, the application of linear wave theory will be more and more pushed to its limits as the wave steepness increases but this is difficult to quantify without the experimental results. Further work aims to apply the available nonlinear functionality in WEC-Sim to the current models.

Appendix A
CCP-WSI Submission Criteria Results

The CCP-WSI submission results can be found in Table IV.

References

[1] CCP-WSI. Focused wave interactions with floating structures (ccp-wsi blind test series 2) — ccp-wsi. [Online]. Available: https://www.ccp-wsi.ac.uk/blind_test_series_2

[2] Y. L. Wu, G. Stewart, Y. Chen, J. Gullman-Strand, X. Lv, and P. Kumar, "A cfd application of newwave theory to wave-in-deck simulation," *International Journal of Computational Methods*, vol. 13, no. 02, p. 1640014, 2016.

TABLE IV
CCP-WSI Blind Test Series 2 Test Cases

		12BT2	11BT2	13BT2	22BT2	21BT2	23BT2
Maximums	Heave displacement (m)	0.0853	0.0956	0.0734	-0.0224	-0.0101	-0.0332
	Surge displacement (m)	0.0862	0.0977	0.0796	0.0880	0.1000	0.0804
	Pitch angle (degrees)	33.986	28.122	38.829	43.538	36.392	47.531
	Mooring load (N)	46.768	47.336	46.185	45.242	46.042	44.524
Preceding trough depth	Heave displacement (m)	-0.2724	-0.2786	-0.2687	-0.3632	-0.3754	-0.3539
	Surge displacement (m)	-0.0683	-0.0661	-0.0667	-0.0691	-0.0661	-0.0685
	Pitch angle (degrees)	-15.672	-12.613	-19.750	-22.614	-19.639	-25.593
	Mooring load (N)	22.491	22.061	22.765	22.373	21.555	22.993
Rising time	Heave displacement (s)	1.0910	1.1938	1.0040	1.1859	1.2965	1.0673
	Surge displacement (s)	1.3361	1.4784	1.2412	1.3361	1.4705	1.2265
	Pitch angle (s)	0.7589	0.7748	0.7352	0.6404	0.6562	0.6166
	Mooring load (s)	1.0831	1.1859	0.9803	1.1779	1.2886	1.0515
Peak frequency	Heave displacement (Hz)	0.4065	0.3599	0.4399	0.4132	0.3532	0.4465
	Surge displacement (Hz)	0.3999	0.3665	0.4265	0.3999	0.3665	0.4332
	Pitch angle (Hz)	0.6531	0.6598	0.6465	0.8197	0.8131	0.8264
	Mooring load (Hz)	0.4065	0.3599	0.4399	0.4132	0.3532	0.4465
Variance density at peak frequency	Heave displacement (m^2/Hz)	0.3098	0.3842	0.2595	0.3100	0.3848	0.2782
	Surge displacement (m^2/Hz)	0.4156	0.5313	0.3106	0.4240	0.5893	0.3161
	Pitch angle (rad^2/Hz)	11696	7935.8	15519	8141.7	5051.9	9490.4
	Mooring load (N^2/Hz)	1365.1	1672.6	1170.7	1391.9	1749.2	1239.6
Spectral bandwidth	Heave displacement (Hz)	0.1463	0.1412	0.1477	0.1558	0.1493	0.1508
	Surge displacement (Hz)	0.1262	0.1228	0.1449	0.1305	0.1150	0.1500
	Pitch angle (Hz)	0.1839	0.1785	0.1807	0.1828	0.1795	0.1888
	Mooring load (Hz)	0.1447	0.1435	0.1423	0.1558	0.1493	0.1506

[3] National Renewable Energy Laboratory and Sandia Corporation, "Wec-sim (wave energy converter simulator) wec-sim documentation," https://wec-sim.github.io/WEC-Sim/index.html, 2015, (Accessed on 19/03/2018).
[4] E. Quon, A. Platt, Y.-H. Yu, and M. Lawson, "Application of the most likely extreme response method for wave energy converters," in *ASME 2016 35th International Conference on Ocean, Offshore and Arctic Engineering*. American Society of Mechanical Engineers, 2016, pp. V006T09A022–V006T09A022.
[5] LHEEA, "Nemoh-presentation - lheea," April 2017, (Accessed on 06/03/2018). [Online]. Available: https://lheea.ec-nantes.fr/logiciels-et-brevets/nemoh-presentation-192863.kjsp
[6] A. Babarit and G. Delhommeau, "Theoretical and numerical aspects of the open source bem solver nemoh," in *11th European Wave and Tidal Energy Conference (EWTEC2015)*, 2015.
[7] M. Penalba, T. Kelly, and J. Ringwood, "Using nemoh for modelling wave energy converters: A comparative study with wamit," 08 2017.
[8] B. Le Méhauté, *An introduction to hydrodynamics and water waves*. Springer Science & Business Media, 2013.
[9] T. Hedges and URSELL, "Regions of validity of analytical wave theories." *Proceedings of the Institution of Civil Engineers-Water Maritime and Energy*, vol. 112, no. 2, pp. 111–114, 1995.
[10] J. Wheeler *et al.*, "Methods for calculating forces produced by irregular waves," in *Offshore technology conference*. Offshore Technology Conference, 1969.
[11] G. Payne, "Guidance for the experimental tank testing of wave energy converters," 2008. [Online]. Available: https://www.ccp-wsi.ac.uk/blind_test_series_2
[12] E. Ransley, D. Greaves, A. Raby, D. Simmonds, and M. Hann, "Survivability of wave energy converters using cfd," *Renewable Energy*, vol. 109, pp. 235–247, 2017.